

Optimal Charging of Valve-Regulated Lead-Acid Batteries Based on Model Predictive Control

Goran Kujundžić^a, Šandor Iles^{b,*}, Jadranko Matuško^b, Mario Vašak^b

^a*Public Enterprise Croatian Telecom JSC, Kneza Branimira bb, 88000 Mostar, Bosnia and Herzegovina.*

^b*University of Zagreb Faculty of Electrical Engineering and Computing, Unska 3, 10000 Zagreb, Croatia.*

Abstract

In this paper an algorithm for optimal charging of a valve-regulated lead-acid (VRLA) battery stack based on model predictive control (MPC) is proposed. The main objective of the proposed algorithm is to charge the battery stack as fast as possible without violating the constraints on the charge current, the battery voltage and the battery temperature. In addition, a constraint on the maximum allowed voltage of every battery in the battery stack is added in order to minimize degradation of the individual batteries during charging. The convexity of the VRLA battery charging optimization problem is proven, which makes the control algorithm suitable for efficient on-line implementation via solving a quadratically constrained quadratic program (QCQP). The recursive feasibility and stability of the proposed control strategy is ensured. The proposed algorithm is validated both through simulation tests and on the experimental setup.

Keywords: valve-regulated lead-acid battery, state of charge, hybrid electrical model, model predictive control

*Corresponding author

Email addresses: goran.kujundzic@hteronet.ba (Goran Kujundžić),
sandor.iles@fer.hr (Šandor Iles), jadranko.matusko@fer.hr (Jadranko Matuško),
mario.vasak@fer.hr (Mario Vašak)

1. Introduction

Valve-regulated lead-acid (VRLA) batteries are used in a wide-range of applications from stand-by power supplies to automotive applications due to their low-cost and high reliability [1, 2]. Their main role in standby applications is to provide energy in the case of power failure. When the power is restored, the battery should be charged as quickly as possible in order to prepare itself for the next power failure [3, 4]. This type of batteries is used in other emerging applications like microgrids, where they are combined with various renewable energy sources [5, 6]. In such cases it proves beneficial to charge the battery as quickly as possible in order to increase gains in optimization of microgrid energy flows. Furthermore, VRLA batteries with a low internal resistance are used in electric and hybrid electric vehicles where they need to be charged as quickly as possible as well [7, 8, 9]. However, fast charging typically comes at the cost of a reduced battery lifetime, which is another important aspect in all the aforementioned applications, since it directly influences the total operating cost of the system due to the fact that battery needs to be replaced periodically [6].

The lifetime of a lead-acid battery is often considered to be a function of materials and design parameters such as grid alloy and thickness, electrolyte composition and strength, as well as the ratio between the quantity of materials constituting the positive and negative electrodes. Besides that, charge and discharge conditions such as rate and depth also have a large impact on lead-acid battery lifetime [10].

There are a few standard charging methods that have been used over the past several decades, regardless of the significant development in technologies from flooded to VRLA batteries [11, 12, 13]. Among them the constant-current (CC), constant-voltage (CV) and constant-current constant-voltage (CCCV) charge methods are considered as the standard charge methods, where the CCCV method is the most commonly used among them [4, 14].

A fast charging can be achieved by using high charge rates and/or high voltage threshold limits [15, 8]. However, in most cases, a fast charging has negative influence on aging factors (water loss, grid corrosion and sulfation of the negative electrode) [4]. Furthermore, when fast charging of VRLA batteries is not adequately controlled, significant damage may occur, ultimately resulting in a reduced battery life. Recharge control strategies which minimize the battery life degradation can be achieved by putting constraints on the battery states such as charge current, the battery voltage, the state-

of-charge and the battery temperature which are typically provided by the battery manufacturer [3, 16, 17, 18]. However, such constraints are rather conservative as they are provided for the complete lifetime of the battery and are typically assumed within the CCCV charging method [19].

In the past 10 years the community recognized the need for advanced control algorithms for battery charging and the battery protection in applications where the battery is used as an energy storage, such as model predictive control (MPC), due to its ability of satisfying battery constraints. At every sampling instant, a finite-horizon optimal control problem is being solved. The current state of the system and a plant model is being used to find an optimal control sequence which results in an optimal behavior of the system which satisfies constraints on control input and states over the finite-horizon. The first control signal in the optimal control sequence is applied to the plant and the whole procedure is repeated in a receding horizon manner [20, 21]. In that way, new developments in the battery modeling and a new knowledge about the influence of the particular battery constraints on the battery lifetime can be exploited in a control design phase in a systematic way.

MPC has been employed in various applications with a battery used as an energy storage. In such applications the battery constraints have been incorporated in the design phase to prolong the battery lifetime. In [22] MPC has been used for demand planning in microgrids while satisfying all the battery constraints. Authors in [23] have used predictive charge control strategy for stationary photovoltaic system with battery storage to reduce the photovoltaic injection into the grid without enlarging the battery size and prolonging the battery lifetime by minimizing the dwell time at high state-of-charge. In [24] authors proposed a combination of the optimal generation scheduling algorithm and MPC which achieved an efficient protection of the VRLA battery bank from deep discharging and overcharging in a microgrid. Also, the papers [6] and [25] have presented MPC algorithm used for optimization of different microgrids with flooded and lithium-ion batteries, respectively, while keeping all the battery states under defined constraints.

MPC has also been used for charging of batteries which are connected directly to the charger. To predict the future battery behaviour, authors in [26] and [27] have used an equivalent circuit model. Authors in [28] used a step-response model as an approximation of the electrochemical model of the battery, while authors in [19] used the full electrochemical model. Using the electrochemical model can result in a better performance compared

to using an equivalent circuit model. However an equivalent circuit model enables for using the standard quadratic MPC framework. In [26] an additional temperature model of the battery is used together with an equivalent circuit model which results in a non-linear MPC problem that is solved using a genetic algorithm. Authors in [29] use MPC to prolong the battery lifetime by using a two-dimensional degradation map which describes battery degradation processes as a function of state-of-charge and charging current. The developed battery model is linearized in order to use the quadratic MPC framework. All the aforementioned papers which are considering a battery connected directly to the charger, apart from [26], provided only simulation results.

From the practical implementation standpoint of the MPC, it is crucial to ensure that the associated optimization problem can be efficiently solved and that a solution exists at every time instant. The latter requirement is usually referred to as the recursive feasibility of an MPC problem. Without recursive feasibility guarantees, MPC algorithm can work perfectly for a while and then suddenly stop because a feasible solution does not exist [20, 21, 30]. This problem is recognized in the case of MPC based battery charging [28], where the constraints are implemented in the form of soft constraints in order to prevent a loss of feasibility. However, by introducing soft constraints, the constraint violation is allowed even for the nominal model. Even if the optimization problem is recursively feasible, MPC does not guarantee stability due to its finite-horizon. The stability has to be ensured in a design phase by using a stabilizing constraints or a properly designed cost function [20, 21]. The aforementioned papers considering MPC based battery charging are missing stability and/or recursive feasibility guarantees. In addition, the papers that are solving a non-linear MPC problem are missing guarantees that their solution is globally optimal.

To bridge this gap, in this paper we propose a non-linear MPC strategy for charging of VRLA batteries which guarantees adherence to all the constraints that are relevant for safe operation of a battery: the upper threshold voltage level, the maximum battery temperature increase - compared to the ambient temperature, the maximum charge current and the maximum state-of-charge. Furthermore, guarantees on the recursive feasibility and stability are enforced for the nominal model of the battery.

Unlike the existing MPC based charging strategies such as [19, 27, 28, 29] the proposed method concentrates on charging of VRLA batteries instead of lithium-ion batteries and provides recursive feasibility and stability guar-

antees. However, the proposed method is not limited solely to charging of VRLA batteries, instead it can be applied for any type of battery represented by an equivalent circuit model. The proposed method is similar to [26] and [27] in the sense that it uses an equivalent circuit model of the battery. In addition, similar to [26] a temperature model of the battery is included which results in a non-linear MPC problem. However, we adopted a temperature model, presented in [31]. Unlike [19, 26, 28] and [29], which also solve a non-linear MPC problem, we prove that our formulation of the non-linear MPC problem is convex and thus we guarantee attaining the global optimum. Furthermore we formulate the nonlinear MPC problem as a convex quadratically constrained quadratic program (QCQP) which can be efficiently solved by the existing solvers.

Since some of the model states are not directly measurable one may use a full-state observer to alleviate that problem. In this paper we rather resort to converting the model to a non-minimal state space form which uses the plant input and outputs as state variables.

The proposed algorithm is validated on a VRLA battery stack both through simulation tests and experimentally. Due to a different behavior of the individual batteries in the battery stack, additional constraints are added to the MPC problem in order to keep the voltage of every battery below the upper threshold voltage level provided by the manufacturer. This additional constraint will cause the MPC algorithm to decrease the charge current if it is expected that the battery voltage of a single battery will increase above the upper threshold voltage level, which causes a slower charging compared to a standard MPC method, but also prolongs the battery life.

This paper is organized as follows: Section 2 presents the models of a VRLA battery together with the experimental setup. The proposed MPC algorithm is presented in Section 3, while Section 4 presents both simulation and experimental results. Section 5 concludes the paper.

2. Battery models and experimental setup

In this paper a hybrid electrical model of a VRLA battery is used for controller design purposes together with a temperature model. In the sequel the aforementioned battery models are presented together with the description of the experimental setup and its parameter identification.

2.1. Hybrid electrical model

Hybrid electrical model of a battery [32] (Fig. 1) is an accurate, intuitive and comprehensive electrical battery model. The model consists of a capacitor ($C_{capacity}$) and a current-controlled current source which models the battery state-of-charge. In addition, similarly to Thevenin based models, the model contains an RC network, which is used for modelling the transient response of the battery. To connect state-of-charge to an open-circuit voltage (V_{OC}), a voltage controlled voltage source is used [32, 33, 34].

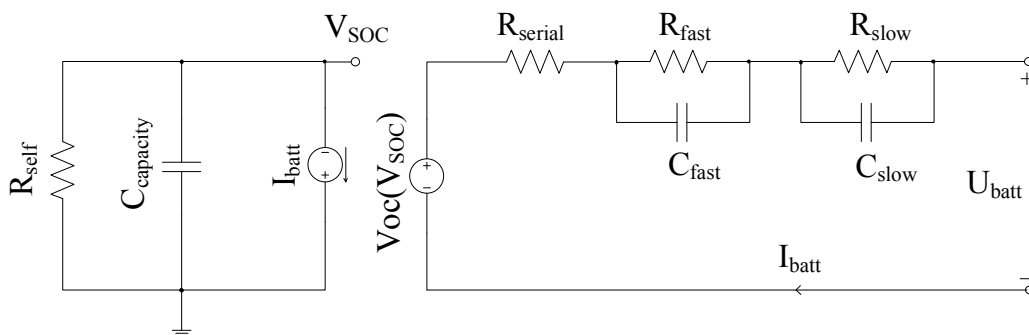


Figure 1: Hybrid electrical model of a battery

To model the battery self-discharge an additional leakage resistor R_{self} can be used in the battery model and it is a function of state-of-charge, temperature and, frequently, number of experienced charge/discharge cycles. The usable capacity presents extracted energy when the battery is discharged from an equally charged state to the same end-of-discharge voltage. The charge of the capacitor $C_{capacity}$ represents the whole charge stored in the battery, i.e., battery state-of-charge. The real capacity of the battery depends on the number of charge/discharge cycles, battery current, ambient temperature and the storage time which has to be taken into account when calculating the battery state-of-charge. It can be calculated by converting the nominal battery capacity in Ahr to charge in Coulomb and its value is defined as [33, 35]:

$$C_{capacity} = 3600Kp_{nom}k_1(cycle)k_2(temp), \quad (1)$$

where Kp_{nom} is a nominal capacity in Ahr, $k_1(cycle)$ is a correction factor for number of charge-discharge cycles, $k_2(temp)$ is an ambient-temperature-dependent correction factor. In this paper the capacity degradation due to

charging with a high current [36] is neglected since the maximum current value is kept below the manufacturer-declared one-hour charge current.

If the self-discharge is neglected, using the Euler-forward discretization with the sampling time T , the hybrid electric model shown in Fig. 1, can be described as the following discrete-time state-space model:

$$\begin{aligned} \begin{bmatrix} V_{OC}(k+1) \\ V_{fast}(k+1) \\ V_{slow}(k+1) \end{bmatrix} &= \begin{bmatrix} 1 & 0 & 0 \\ 0 & 1 - \frac{T}{R_{fast}C_{fast}} & 0 \\ 0 & 0 & 1 - \frac{T}{R_{slow}C_{slow}} \end{bmatrix} \begin{bmatrix} V_{OC}(k) \\ V_{fast}(k) \\ V_{slow}(k) \end{bmatrix} + \\ &+ \begin{bmatrix} \frac{-aT}{C_{capacity}} \\ \frac{T}{C_{fast}} \\ \frac{T}{C_{slow}} \end{bmatrix} I_{batt}(k), \end{aligned} \quad (2)$$

where the battery terminal voltage U_{batt} is given as follows:

$$U_{batt}(k) = V_{OC}(k) - V_{fast}(k) - V_{slow}(k) - R_{serial}I_{batt}(k), \quad (3)$$

and V_{serial} , V_{fast} , V_{slow} and V_{OC} are voltages at serial resistor, fast and slow-transient RC parallel network and the open-circuit voltage, respectively and the battery current is assumed negative during charging.

In general, state-of-charge (*SOC*) has a non-linear dependence on the open-circuit voltage. However for simplicity in this paper we use the following approximation which is often used in the literature [11, 37, 38, 39]:

$$SOC(k) = \frac{100}{a}V_{OC}(k) - \frac{100b}{a}, \quad (4)$$

where b is the open-circuit-voltage of an empty battery, while $a + b$ is the open-circuit-voltage of a full battery. If a better accuracy of the model is needed a piece-wise affine approximation can be used.

More details on the the hybrid electrical model and its validation using different charge and discharge currents, at different ambient temperatures can be found in [32].

2.2. Temperature model of a VRLA battery

The ambient and battery temperatures are very important parameters during the charging of a VRLA battery. These parameters define how long the battery can be charged with defined current rates without damaging it and reducing its life cycle. The actual value of the battery temperature

is not known because VRLA batteries are sealed, and it is not possible to insert the thermometer inside them. The temperature inside the battery is not spatially uniform, but rather varies depending on the position in the electrolyte. However, the temperature deviation from the mean value is not significant, and accordingly, in this paper, it is assumed that the temperature inside the battery has a uniform spatial distribution. Many researchers have used measurements to determine the temperature outside of the battery that most accurately indicates the temperature inside the battery cells. Dieter in [40] measured the ambient temperature, the temperature of the battery case and the temperatures of the positive and negative terminals during charging of VRLA GEL 6 V, 160 Ah battery with current of 30 A. The measurements showed that the negative terminal temperature had the highest value and that it was the closest to the inner cell temperature. Authors in [41] have measured inner battery temperature using a thermometer inserted during manufacturing of the battery. The temperatures were monitored on the surface of the negative and positive terminals, both end cell container walls (parallel to the plates), a middle cell container wall and inside the cell at the top surface of a plate. After measuring with various charge rates, it has been shown that all the external temperatures followed the battery and the cell temperature very well.

The battery temperature increases from the initial temperature to the final temperature in an exponential fashion during the charging. The initial battery temperature is equal or close to the ambient temperature. The final battery temperature is a function of the charge current, the Joule heating and charge thermal factor which presents heat generation during the charging [31, 42].

Assuming that the ambient temperature is a constant, the discrete-time temperature model for charging of VRLA battery is represented as follows [31]:

$$\begin{aligned} \begin{bmatrix} T_{batt}(k+1) \\ T_a(k+1) \end{bmatrix} &= \begin{bmatrix} (1-Q_T) & Q_T \\ 0 & 1 \end{bmatrix} \begin{bmatrix} T_{batt}(k) \\ T_a(k) \end{bmatrix} + \\ &+ \begin{bmatrix} K_T \\ 0 \end{bmatrix} I_{batt}^2(k), \end{aligned} \quad (5)$$

where Q_T is the charge thermal factor, K_T is the Joule heating factor, I_{batt} is the charge current and T_a is the ambient temperature.

2.3. Experimental setup

Fig. 2 shows a principal scheme of the test system designed for charging of the VRLA 48 V battery stack, with a nominal capacity 45 Ah. It consists of four 12 V Ritar [43] batteries connected in series. The battery monitoring system consists of an acquisition card based on Microchip PIC18F2550, which is used for measuring each 12 V battery voltages, the overall battery stack voltage, the charge/discharge current, the temperature of the battery stack negative terminal and the ambient temperature. Besides the acquisition card, the battery monitoring consists of the corresponding voltage sensors, the current transformer and two temperature sensors. Error tolerances for the measurement system components are given in Tab. 1, where SOC is estimated by integrating the battery current over time with SOC initial value calculated based on the open-circuit-voltage. DC 48 V Delta charger with the PSC 3 controller [44] is used for charging. The communication between PC and the controller is established using an additionally designed computer program.

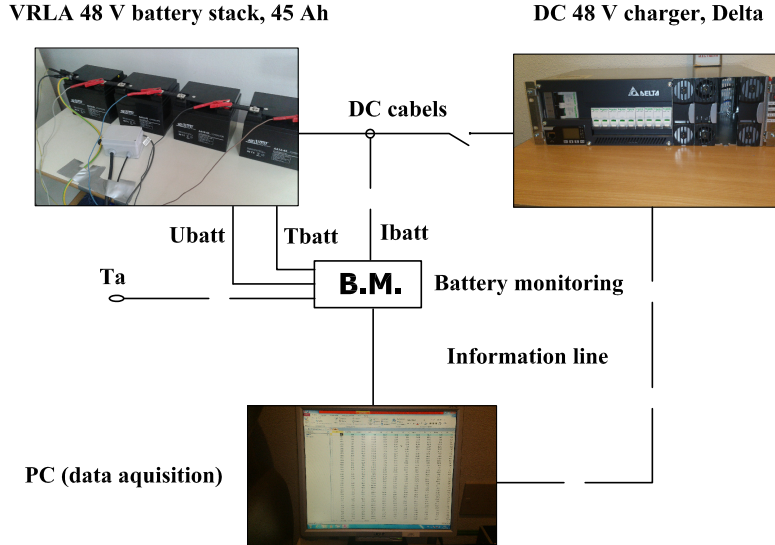


Figure 2: Experimental test system

2.4. Battery model parameters identification

To determine the open-circuit voltage (V_{OC}) and the battery parameters (R_{serial} , R_{fast} , R_{slow} , C_{fast} , and C_{slow}), the charge/discharge test was carried

Table 1: Error tolerances of the measurement system

Quantity	Range	Maximum error
Battery voltage	7 V DC - 18 V DC	± 0.5 mV
Battery current	2 A DC - 65 A DC	± 65 mA
Battery current	0.5 A DC - 2 A DC	± 120 mA
Battery temperature	13.5 °C - 18°C	± 0.005 °C
Battery temperature	18°C - 25°C	± 0.018 °C
Battery temperature	25°C - 33°C	± 0.025 °C
Battery temperature	33°C - 40°C	± 0.030 °C

out using the battery stack with the 10-hour charge/discharge current recommended by the manufacturer. A Fuguang DC variable resistor was used for discharging in the experimental test system. At first, the battery stack was discharged from a fully charged state. The discharge period of 60 minutes was altered with the resting period of 20 minutes. Similar pulse current strategy was applied for charging of the battery stack. The threshold voltage levels, provided by the manufacturer are used for stopping of the charging and discharging processes.

The battery voltage tends to its open-circuit voltage after charge/discharge current decreases to a near-zero value. The open-circuit voltage is normally measured as a steady-state battery open-circuit voltage at various *SOC* points. However, for each *SOC* point this measurement can take days. The rapid method [45] for determining the open-circuit voltage parameters (a , b) are used and the obtained values are given in Tab. 2.

The battery parameters (R_{serial} , R_{fast} , R_{slow} , C_{fast} , and C_{slow}) are analytically calculated from the corresponding voltage-time curves of the aforementioned charge/discharge tests.

In order to improve steady-state accuracy of the model R_{serial} , R_{fast} , R_{slow} are further estimated by using a Sigma-point Kalman Filter (SPKF), with their analytically calculated values used as the initial guesses for the estimation process. The parameter estimation is performed only once before experimental tests. More on the estimation procedure used in this paper can be found in [46]. The estimated values of the battery parameters are given

Table 2: Parameters of the hybrid electrical model

Symbol	Description	Value
R_{serial}	Serial resistor	0.1635 Ω
R_{fast}	Fast-transient resistor	0.0806 Ω
R_{slow}	Slow-transient resistor	0.0465 Ω
$C_{capacity}$	Battery capacitor	129600 F
C_{fast}	Fast-transient capacitor	3400 F
C_{slow}	Slow-transient capacitor	89145 F
a	Open-circuit voltage parameter	7.70
b	Open-circuit voltage parameter	44.00 V

Table 3: Parameters of temperature model of the battery

Symbol	Description	Value
Q_T	Charge thermal factor	0.0017
K_T	Joule heating factor	1.416210^{-4}

in Tab. 2.

The coefficients (Q_T , K_T), of the temperature model (5) are identified from the experimental data obtained by charging of the battery stack with two current rates (14 A and 18 A) using CCCV charge algorithm. The experimental data is sampled with the sampling time $T = 1$ min. Using the Constrained Linear Least Squares (CLS) method [47], the coefficients of the temperature model are obtained and given in Tab. 3.

To account for a possible change of the parameters caused by aging of the battery parameters can be updated based on the data collected after each charging or they can be updated during charging using SPKF. However, in this paper results are shown for constant parameter values.

2.5. Validation of the battery parameters

In order to validate the parameters of the equivalent circuit model and the temperature model a comparison between the measured data and the data obtained by the model during pulse charging with the current 18 A is shown in Fig. 3.

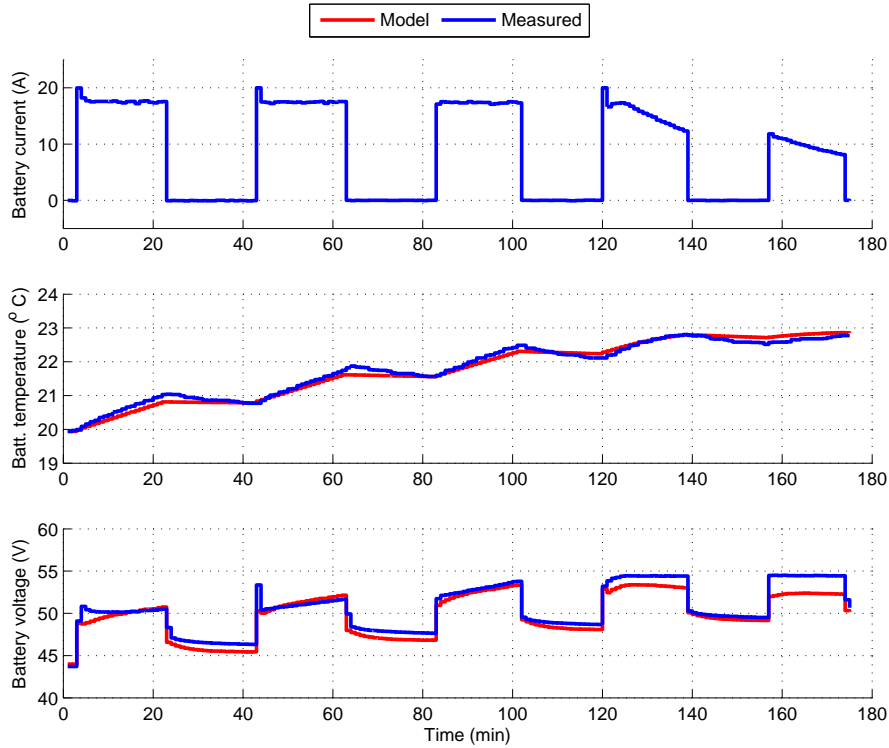


Figure 3: Validation of the hybrid electrical model and temperature model during pulse charging

The presented results show that there exists a discrepancy between the model and the experimental setup which is especially visible at high levels of *SOC*.

More details on parameter identification and model validation can be found in [46] where the parameters of a similar battery are identified and it is shown that there exists a discrepancy between the hybrid electrical model and the experimental setup at low levels of *SOC* as well.

3. Model predictive control for battery charging

Model predictive control is a control strategy where at each sampling instant one solves a finite horizon optimal control problem over the future behaviour of the system which is obtained using a model of the plant and the initial state of the system. At each sampling instant an optimal control input sequence is obtained and the first control input is applied to the plant. The whole process is then repeated in a receding horizon manner [20].

A typical objective function in model predictive control often provides some trade-off between the tracking error and the control input. Therefore the objective function is chosen as follows:

$$J(x(k), I(k)) = \sum_{j=0}^{N-1} ((100 - SOC(k+j)) - \lambda I(k+j)) + P(100 - SOC(k+N)), \quad (6)$$

where $\lambda \geq 0$ is a tuning parameter and $P \geq 0$ is the weight on the terminal cost.

However, in the case of battery charging, a typical objective of the optimization is to charge the battery as fast as possible without violating the constraints in order to prolong the battery life. However minimum-time problems are difficult to solve in practice. In the literature it has been shown that standard MPC cost function with a low weight on the control input and $P = 1$ results in a pseudo-minimum time battery charging [27]. Therefore to approximate the minimum time charging the parameter λ can be set to zero or a very small positive value.

The current is constrained to only allow charging of the battery with the admissible charge current:

$$-I_{battmax} \leq I_{batt}(k+j) \leq 0, \quad j = 0, \dots, N-1. \quad (7)$$

The battery voltage must be constrained below the maximum allowed value provided by the manufacturer as follows:

$$U_{batt}(k+j) \leq U_{battmax}, \quad j = 0, \dots, N-1. \quad (8)$$

However, it is important to note that according to (3) the battery terminal voltage depends directly on the applied current. Since the terminal voltage is measured before applying the optimal value of current, measured value of the battery terminal voltage $\tilde{U}_{batt}(k)$ depends on the current as follows:

$$\tilde{U}_{batt}(k) = V_{OC}(k) - V_{fast}(k) - V_{slow}(k) - R_{serial}I_{batt}(k-1). \quad (9)$$

For that reason the following constraint is also added to the optimization problem.

$$\tilde{U}_{batt}(k+j) \leq U_{battmax}, j = 1, \dots, N. \quad (10)$$

to ensure satisfaction of the voltage constraint for the whole interval $[k+j, k+j+1)$.

To prevent overcharging of the battery the maximum *SOC* is constrained below 100%:

$$SOC(k+j) \leq 100\%, j = 1, \dots, N. \quad (11)$$

To prevent overheating and thermal runaway of the battery it is necessary to control the battery temperature during charging. This goal can be achieved by imposing a constraint on the maximum temperature increase $\Delta T_{battmax}$ above the ambient temperature T_a :

$$T_{batt}(k+j) \leq \Delta T_{battmax} + T_a, j = 1, \dots, N, \quad (12)$$

or by imposing a constraint on the maximum allowed temperature of the battery $T_{battmax}$ as follows:

$$T_{batt}(k+j) \leq T_{battmax}, j = 1, \dots, N. \quad (13)$$

Both parameters $T_{battmax}$ and $\Delta T_{battmax}$ can be adapted if necessary during charging.

In order to satisfy the aforementioned constraints, model predictive control with the above mentioned cost and constraints, the hybrid electrical model (2)-(4) and temperature model (5) is used. To predict the future behaviour, the electrical model of the battery requires information about the battery *SOC*, the battery voltage U_{batt} and the voltages V_{fast} and V_{slow} . However, the only measurable variable is the battery voltage \tilde{U}_{batt} , while the *SOC* is estimated by integrating the battery current over time with its initial value calculated based on the open-circuit-voltage. The control input is the battery current $I_{batt}(k)$. In order to avoid having a full state observer which would complicate stability and feasibility analysis [48, 49], the hybrid electrical model (2) is converted to a non-minimal state space realization which uses previous values of the plant input and outputs as state variables. In that way, only the past values of the battery voltage and the battery current are needed to predict the future behaviour of the battery. However, this requires storing the battery terminal voltage and current into computer memory to

initialize the algorithm. The non-minimal state space model is for brevity denoted as:

$$x_1(k+1) = A_1 x_1(k) + B_1 u(k), \quad (14)$$

where $u(k) = I_{batt}(k)$ and

$$x_1(k) = \begin{bmatrix} SOC(k) \\ \tilde{U}_{batt}(k) \\ \tilde{U}_{batt}(k-1) \\ \tilde{U}_{batt}(k-2) \\ I_{batt}(k-1) \\ I_{batt}(k-2) \\ I_{batt}(k-3) \end{bmatrix}, \quad A_1 = \begin{bmatrix} 1 & 0 & 0 & 0 & 0 & 0 & 0 \\ 0 & -a_2 & -a_1 & -a_0 & b_2 & b_1 & b_0 \\ 0 & 1 & 0 & 0 & 0 & 0 & 0 \\ 0 & 0 & 1 & 0 & 0 & 0 & 0 \\ 0 & 0 & 0 & 0 & 0 & 0 & 0 \\ 0 & 0 & 0 & 0 & 1 & 0 & 0 \\ 0 & 0 & 0 & 0 & 0 & 1 & 0 \end{bmatrix}, \quad B_1 = \begin{bmatrix} K \\ b_3 \\ 0 \\ 0 \\ 1 \\ 0 \\ 0 \end{bmatrix}, \quad (15)$$

$$K = -100 \frac{T}{C_{capacity}}, \quad K_1 = \frac{T}{C_{fast}}, \quad K_2 = \frac{T}{C_{slow}}, \quad \tilde{K} = K \frac{a}{100},$$

$$z_1 = \left(1 - \frac{T}{R_{fast} C_{fast}}\right), \quad z_2 = \left(1 - \frac{T}{R_{slow} C_{slow}}\right),$$

$$a_0 = -z_1 z_2, \quad a_1 = z_1 + z_2 + z_1 z_2, \quad a_2 = -(1 + z_1 + z_2),$$

$$b_0 = R_{serial} z_1 z_2, \quad b_1 = \tilde{K} z_1 z_2 - K_2 z_1 - R_{serial} z_1 - R_{serial} z_2 - K_1 z_2 - R_{serial} z_1 z_2,$$

$$b_2 = K_1 + K_2 + R_{serial} + K_1 z_2 + K_2 z_1 - \tilde{K} z_1 - \tilde{K} z_2 + R_{serial} z_1 + R_{serial} z_2,$$

$$b_3 = \tilde{K} - K_2 - K_1 - R_{serial}$$

In a similar way, the non-linear discrete-time temperature model (5) is denoted as follows:

$$x_2(k+1) = A_2 x_2(k) + B_2 u^2(k), \quad (16)$$

where $x_2(k) = [T_{batt}(k) \quad T_a(k)]^T$, and the corresponding matrices A_2 and B_2 are given in (5).

The battery charging optimization problem can be written in the following form:

$$\begin{aligned}
& \min_U \sum_{j=0}^{N-1} ((100 - SOC(k+j)) - \lambda u(k+j)) + P(100 - SOC(k+N)) \\
& \text{s.t. } x_1(k+j+1) = A_1 x_1(k+j) + B_1 u(k+j), j = 0, \dots, N-1, \\
& \quad x_2(k+j+1) = A_2 x_2(k+j) + B_2 u^2(k+j), j = 0, \dots, N-1, \\
& \quad z(k+j) = Fx(k+j) + Gu(k+j), j = 0, \dots, N-1 \\
& \quad u(k+j) \in \mathcal{U}, j = 1, \dots, N-1 \\
& \quad x_1(k+j) \in \mathcal{X}_1, j = 0, \dots, N \\
& \quad x_2(k+j) \in \mathcal{X}_2, j = 0, \dots, N \\
& \quad z(k+j) \in \mathcal{H}, j = 0, \dots, N-1, \\
& \quad x_1(k+N) \in \mathcal{X}_{T1},
\end{aligned} \tag{17}$$

where $SOC(k+j) = [1 \ 0 \ 0 \ 0 \ 0 \ 0 \ 0] x_1(k)$, U denotes the control input sequence as follows:

$$U = [u(k) \ \dots \ u(k+N-1)]^T \tag{18}$$

and sets \mathcal{X}_1 , \mathcal{X}_2 are polyhedral sets representing the state constraints, \mathcal{U} is a polyhedral set representing the input constraint, while \mathcal{H} is a polyhedral set representing joint state-input constraints. The sets are defined as follows:

$$\mathcal{X}_1 = \{x : H_1 x \leq M_1\}, \tag{19}$$

$$\mathcal{X}_2 = \{x : H_2 x \leq M_2\}, \tag{20}$$

$$\mathcal{U} = \{u : H_3 u \leq M_3\}, \tag{21}$$

$$\mathcal{H} = \{z : H_4 z \leq M_4\}, \tag{22}$$

where

$$F = [0 \ 1 \ 0 \ 0 \ R_{serial} \ 0 \ 0], G = -R_{serial}, \tag{23}$$

$$H_1 = \begin{bmatrix} 1 & 0 & 0 & 0 & 0 & 0 & 0 \\ 0 & 1 & 0 & 0 & 0 & 0 & 0 \end{bmatrix}, M_1 = \begin{bmatrix} 100 \\ U_{battmax} \end{bmatrix}, \tag{24}$$

$$\tag{25}$$

$$H_2 = \begin{bmatrix} 1 & -1 \\ 1 & 0 \end{bmatrix}, M_2 = \begin{bmatrix} \Delta T_{battmax} \\ T_{battmax} \end{bmatrix}, \quad (26)$$

$$H_3 = \begin{bmatrix} 1 & 0 \\ 0 & -1 \end{bmatrix}, M_3 = \begin{bmatrix} 0 \\ I_{battmax} \end{bmatrix} \quad (27)$$

$$H_4 = 1, M_4 = U_{battmax}. \quad (28)$$

The sets and $\mathcal{X}_{T1} \subseteq \mathcal{X}_1$ and \mathcal{X}_2 are positively invariant polyhedral sets under a stabilizing control law

$$u(k) = C(100 - SOC(k)) \quad (29)$$

where $C(100 - SOC(k)) \in \mathcal{U}, \forall x_1 \in \mathcal{X}_{T1}$ and C is a negative scalar in the following interval:

$$-\frac{1}{100} \sqrt{\frac{\min(\Delta T_{battmax}, T_{battmax} - T_a) Q_T}{K_T}} \leq C < 0. \quad (30)$$

The set \mathcal{X}_{T1} is defined as follows

$$\mathcal{X}_{T1} = \{x : H_{T1}x \leq M_{T1}\}, \quad (31)$$

where H_{T1} and M_{T1} are computed using the system dynamics (14) with the stabilizing control law (29).

Remark: The optimization problem can easily be extended for charging a battery stack by augmenting the optimization problem as follows

$$\begin{aligned} x_{1,i}(k+j+1) &= A_{1i}x_{1,i}(k+j) + B_{1i}u(k+j), j = 0, \dots, N-1, \\ z_{1,i}(k+j) &= Hx_{1,i}(k+j) + Fu(k+j), j = 0, \dots, N-1 \\ x_{1,i}(k+j) &\in \mathcal{X}_{1,i}, j = 1, \dots, N, \\ z_{1,i}(k+j) &\in \mathcal{H}_i, j = 0, \dots, N-1, \\ x_{1,i}(k+N) &\in \mathcal{X}_{T1,i}, \end{aligned} \quad (32)$$

where i is an index representing a battery in the battery stack, $x_{1,i}$, A_{1i} and B_{1i} represents the states and the corresponding matrices in the hybrid electrical model (15) respectively, where the battery parameters are computed under assumption that four batteries connected in series result in a hybrid electrical model with parameters given in Tab 2. The sets $\mathcal{X}_{1,i}$, \mathcal{H}_i represents

modified sets of state and joint state-input constraints for each battery while $\mathcal{X}_{T1,i}$ represents the corresponding positively invariant set subject to terminal control law (29).

Clearly the optimization problem (17) is non-linear due to the non-linear temperature model (5) of the battery. However, in the next subsection we show that the optimization problem is convex, and thus its solving can be performed efficiently.

3.1. Convexity of the battery charging optimization problem

In order to show the convexity of the optimization problem (17) the problem is rewritten in a so called batch dynamics form. Let $O_{m \times n} \in \mathbb{R}^{m \times n}$ denotes a zero matrix and let us introduce the following matrices:

$$\tilde{A}_{1j} = [A_1^{j-1} B_1 \dots A_1 B_1 B_1 O_{7 \times \max(0, N-j)}], \quad (33)$$

$$\tilde{A}_{2j} = [A_2^{j-1} B_2 \dots A_2 B_2 B_2 O_{2 \times \max(0, N-j)}]. \quad (34)$$

Then the states $x_1(k+j)$ and $x_2(k+j)$ can be written in the batch dynamics form as a function of the input sequence and the initial state as follows:

$$x_1(k+j) = A_1^j x_1(k) + \tilde{A}_{1j} [u(k) \dots u(k+N-1)]^T, \quad (35)$$

$$x_2(k+j) = A_2^j x_2(k) + \tilde{A}_{2j} [u^2(k) \dots u^2(k+N-1)]^T. \quad (36)$$

Both state constraints $x_1(k+j) \in \mathcal{X}_1$ and terminal constraint $x_1(k+N) \in \mathcal{X}_{T1}$ for the hybrid electrical model are represented by a polyhedral set. Therefore convexity analysis is the same for both sets. By substituting the batch dynamics into the state constraints for the hybrid electrical model, the following expression is obtained:

$$H_1 A_1^j x_1(k) + H_1 \tilde{A}_{1j} U \leq M_1. \quad (37)$$

The constraint (37) is affine in U and therefore convex. In a similar way, by substituting the batch dynamics into the the temperature model constraints (25) the following expression is obtained:

$$H_2 A_2^j x_2(k) + H_2 \tilde{A}_{2j} [u^2(k) \dots u^2(k+N-1)]^T \leq M_2. \quad (38)$$

Due to the upper-triangular structure of the matrix A_2 , the following expression holds:

$$\begin{aligned} D &= [1 \ 0] H_2 \tilde{A}_{2j} = [0 \ 1] H_2 \tilde{A}_{2j} = \\ &= K_T [(1 - Q_T) \ (1 - Q_T)^2 \ \dots \ (1 - Q_T)^j]. \end{aligned} \quad (39)$$

Therefore, the constraints for the temperature model (38) can be written as follows:

$$\begin{bmatrix} 1 & 0 \end{bmatrix} H_2 A_2^j x_2(k) + U^T \text{Diag}(D) U \leq \begin{bmatrix} 1 & 0 \end{bmatrix} M_2, \quad (40)$$

$$\begin{bmatrix} 0 & 1 \end{bmatrix} H_2 A_2^j x_2(k) + U^T \text{Diag}(D) U \leq \begin{bmatrix} 0 & 1 \end{bmatrix} M_2, \quad (41)$$

where Diag denotes an operator returning a diagonal matrix with diagonal terms formed from the vector given as its argument. The constraints (40) and (41) are convex since D is positive semidefinite due to the fact that $Q_T \in [0, 1)$ and $K_T > 0$.

The input constraint $u(k+j) \in \mathcal{U}$ can be written as follows

$$H_3 e_j U \leq M_3, \quad (42)$$

where $e_j = [O_{1 \times j} \ 1 \ O_{1 \times N-j-1}]$ and therefore it is convex.

The mixed state-input constraint $z(k+j) \in \mathcal{H}$ can be written as follows

$$H_4 (F A_1^j x_1(k) + (F \tilde{A}_{1j} + G e_j) U) \leq M_4, \quad (43)$$

which is also affine in U and therefore convex.

The cost function (6) can be written as an affine function of the input sequence:

$$\begin{aligned} J(x(k), U) = & \sum_{j=1}^{N-1} (100 - [1 \ 0 \ 0 \ 0 \ 0 \ 0 \ 0] (A_1^j x_1(k) + \tilde{A}_{1j} U)) - \lambda e_j U + \\ & + P(100 - [1 \ 0 \ 0 \ 0 \ 0 \ 0 \ 0] (A_1^N x_1(k) + \tilde{A}_{1N} U)), \end{aligned} \quad (44)$$

therefore the proposed model predictive control problem is convex. Furthermore, it can be written as a convex QCQP which can be efficiently solved by the existing solvers.

3.2. Recursive feasibility of the battery charging optimization problem

From the practical implementation standpoint one of the main issues when solving an MPC optimization problem online is to ensure that the optimization problem will have a solution at every time instant, i.e started from initially feasible state the optimization problem will be feasible at any future time instant. This property is usually referred to as the recursive feasibility of an MPC problem [20, 30].

Given an initial feasible pair $x_1(k)$ and $x_2(k)$ at the time step k , there exists the optimal sequence

$$U^*(k) = [u^*(k|k) \quad u^*(k+1|k) \quad \dots \quad u^*(k+N-1|k)], \quad (45)$$

leading to a state-trajectory for the hybrid electrical model and the temperature model of the battery respectively:

$$X_1^*(k) = [x_1^*(k|k) \quad x_1^*(k+1|k) \quad \dots \quad x_1^*(k+N-1|k)], \quad (46)$$

$$X_2^*(k) = [x_2^*(k|k) \quad x_2^*(k+1|k) \quad \dots \quad x_2^*(k+N-1|k)]. \quad (47)$$

At the next time step the following holds: $x_1(k+1) = x_1^*(k+1|k)$ and $x_2(k+1) = x_2^*(k+1|k)$. Since the terminal set \mathcal{X}_{T1} and the set \mathcal{X}_2 are positively invariant subject to the control law (29) and $C(100 - SOC(k)) \in \mathcal{U}, \forall x_1 \in \mathcal{X}_{T1}$, the sequence

$$\begin{aligned} U_{feasible}(k+1) &= \\ &= [u^*(k+1|k) \quad \dots \quad u^*(k+N-1|k) \quad C(100 - SOC^*(k+N|k))] \end{aligned} \quad (48)$$

is a feasible sequence at the time step $k+1$, where

$$SOC^*(k+N|k) = [1 \quad 0 \quad 0 \quad 0 \quad 0 \quad 0 \quad 0] x_1^*(k+N|k).$$

Therefore the optimization problem (17) is recursively feasible.

To show that the corresponding optimization problem is stabilizing we show that the proposed cost function

$$\begin{aligned} J(x(k), U^*(k)) &= \sum_{j=0}^{N-1} ((100 - SOC^*(k+j|k)) - \lambda u^*(k+j|k)) + \\ &+ P(100 - SOC^*(k+N|k)) \end{aligned} \quad (49)$$

is a Lyapunov function. Since the current $u(k+j) \leq 0$ and $SOC(k+j) \in [0, 100]$, the objective function is a positive definite function. It is constrained from below as follows:

$$100 - SOC(k) \leq J(x(k), U^*(k)). \quad (50)$$

From (14) and (15) it follows that

$$SOC(k+1) = SOC(k) + Ku(k), \quad (51)$$

where $K < 0$. Since $SOC(k + j) \leq 100$ the following condition holds $0 \leq u(k) \leq \frac{1}{K}(100 - SOC(k))$. It follows that $J(x(k), U^*(k)) \leq ((N - 1)(1 - \frac{\lambda}{K}) + P)(100 - SOC(k))$. Therefore

$$(100 - SOC(k)) \leq J(x(k), U^*(k)) \leq \beta(100 - SOC(k)). \quad (52)$$

where $\beta = ((N - 1)(1 - \frac{\lambda}{K}) + P) > 1$.

The optimal value of the cost function at the time step k is $J(x(k), U^*(k))$. At the time step $k + 1$ the optimal value of the cost function is smaller or equal to $J(x^*(k + 1|k), U_{feasible}(k + 1))$. Therefore the following holds

$$\begin{aligned} \Delta J &= J(x^*(k + 1|k), U^*(k + 1)) - J(x^*(k|k), U^*(k)) \leq \\ &- (100 - SOC(k) - \lambda u^*(k|k)) - P(100 - SOC(k + N)) + \\ &+ (100 - SOC(k + N))(1 - \lambda C + P(1 - KC)) \end{aligned} \quad (53)$$

If P is chosen as follows

$$P = \frac{1 - \lambda C}{KC} \quad (54)$$

$$\Delta J \leq -(100 - SOC(k)), \quad (55)$$

exponential stability is ensured.

However, due to the nature of the hybrid electrical model a less conservative P can be chosen. If $SOC(k + N) < 100$ the following condition holds

$$100 - SOC(k) \leq 100 - SOC(k + N) < (100 - SOC(k + N))(1 - KC), \quad (56)$$

$$\begin{aligned} \Delta J &< - (100 - SOC(k + N)(1 - KC)) - P(100 - SOC(k + N)) + \\ &+ (100 - SOC(k + N))(1 - \lambda C + P(1 - KC)) \end{aligned} \quad (57)$$

A sufficient condition for negativity of (57) is

$$P \geq \frac{K - \lambda}{K}. \quad (58)$$

If $SOC(k + N) = 0$ then

$$\Delta J \leq -(100 - SOC(k)), \quad (59)$$

and therefore $\lim_{j \rightarrow \infty} SOC(k + j) = 100$.

If $\lambda = 0$, the terminal set constraint can be omitted if $V_{fast}(k) \leq 0$, $V_{slow}(k) \leq 0$ and $u(k-1) \leq 0$. In this case $u(k+j) = 0$, $j = 0, \dots, N-1$ is a feasible control sequence if $x_1(k) \in \mathcal{X}_1$ and $x_2(k) \in \mathcal{X}_2$. According to the battery temperature model (5) and hybrid electrical model (2)-(4), the control sequence $u(k+j) = 0$ ensures that the battery *SOC* remains unchanged while both, the battery temperature and voltage, exponentially decay towards the ambient temperature T_a and the open-circuit-voltage V_{OC} , respectively. Therefore the system states evolve inside the set \mathcal{X}_1 and \mathcal{X}_2 respectively. Furthermore mixed state-input constraint is also satisfied with $u(k+j) = 0$ since $u(k-1) \leq 0$ and the battery voltage at time step $k+j$ can be calculated from the measured battery voltage as follows $U_{batt}(k+j) = \tilde{U}_{batt}(k+j) + R_{serial}(u(k+j-1) - u(k+j))$ and consequently $U_{batt}(k+j) \leq \tilde{U}_{batt}(k+j)$ and the optimization problem (17) is recursively feasible. Furthermore $\forall x_2 \in \mathcal{X}_2$ and $\forall x_1(k) \in \text{int}(\mathcal{X}_1)$ where *int* denotes strict interior of the set, besides the control sequence $u(k+j) = 0$ there also exists a feasible control sequence where the first element is some value from the interval $-I_{batt_{max}} \leq u(k) < 0$ which keeps the system states x_1 and x_2 inside the sets \mathcal{X}_1 and \mathcal{X}_2 respectively. Since the first element of the sequence $u(k) < 0$ is feasible in the interior of the set \mathcal{X}_1 , the *SOC* increases and as a consequence the cost function (44) decreases. Let us now consider the case when the system states x_1 lie on the border of the feasible sets \mathcal{X}_1 . If *SOC* = 100% the control sequence $u(k+j) = 0$ is the optimal control sequence and the battery is fully charged. In the case when *SOC* < 100%, the control sequence $u(k+j) = 0$ will drive the states of the battery temperature towards the ambient temperature T_a and the battery terminal voltage towards the open-circuit-voltage V_{oc} which lie in the interior of the sets \mathcal{X}_1 . In the interior, a sequence with first element $u(k) < 0$ becomes feasible which results in charging of the battery. Therefore *SOC* converges to 100%.

In the sequel the simulation and experimental results are presented.

4. Simulation and Experimental Results

The proposed MPC algorithm (17) is implemented in Matlab using Yalmip and Sedumi optimization software [50, 51] and it is tested both in simulation and in the experimental setup (Fig. 2). The corresponding terminal set is computed using MPT toolbox [52]. When computing the terminal set it is sufficient to take into account state and input constraints since the joint state-input constraint is automatically satisfied due to the form of terminal

control law (29). The prediction horizon N is selected to be equal to the control horizon. Since the terminal constraint is used as a stabilizing ingredient an increase of the prediction horizon may lead to a larger feasible set and therefore to a better performance. However, increasing the prediction horizon contributes to an increased computational burden. Therefore the prediction horizon N can be seen as a tuning parameter between the computational burden and the control performance. Numerical values of MPC parameters are shown in Tab. 4, while the corresponding terminal set is shown in Fig 4.

Since stationary VRLA batteries with thick electrodes have been used in the experimental setup under normal operating conditions, the maximum permitted increase of the battery temperature $\Delta T_{battmax}$ is set to a value below 10°C in all the experiments to prevent the thermal runaway of the battery [18]. However, the temperature constraint can be selected to be different according to the battery technology and operating conditions.

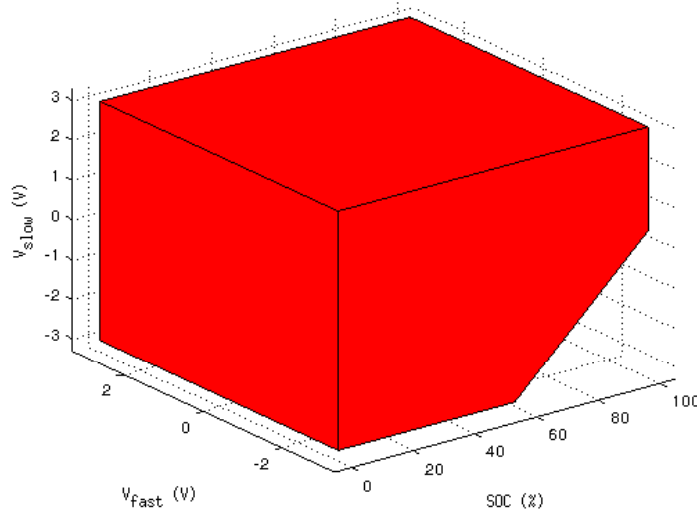


Figure 4: Terminal set: A positively invariant set for the system (14) subject to the control law (29)

The simulation and experimental results of charging VRLA battery stack using the MPC algorithm with $\Delta T_{battmax} = 7^\circ\text{C}$ are given in figures 5 and 6 where battery voltage U_{batt} , the charge current I_{batt} , the battery temperature T_{batt} , and the battery SOC are shown.

Table 4: Parameters of model predictive control algorithm

Symbol	Description	Value
N	Prediction horizon	5
$I_{battmax}$	Current constraint	17.20 A
$U_{battmax}$	Voltage constraint	54.50 V
$SOC_{battmax}$	SOC constraint	100%
λ	Control input weight	0
P	Terminal cost weight	1
C	Terminal control law gain	-10^{-6}

Charging of the battery using the proposed MPC algorithm took 129 minutes in simulation and 134 minutes in the experiment. This difference is partly a consequence of the discrepancy between the battery model (2) and the experimental setup. In both cases the battery temperature is below the maximum allowed temperature of the battery.

During charging (figures 5 and 6) the battery temperature did not reach the temperature constraint. However, in general, the temperature constraint is important during battery charging [28] especially if high charging current is used. To demonstrate that the proposed algorithm is capable of keeping the battery temperature below the maximum allowed value a maximum charging current can be increased or the temperature limit can be decreased. We chose the latter approach and set $\Delta T_{battmax}$ to 3.5 °C. The simulation and experimental results are shown in figures 7 and 8, respectively.

During experimental test shown in Fig 8 when the constraint on the maximum temperature is active, the algorithm decreases the current to keep the battery temperature on the corresponding limit. However, due to discrepancy between the model and the experimental setup the battery temperature decreases below the maximum allowed temperature and a higher charging current is allowed for a short period of time which results in a reduced charging time compared to simulation (Fig 7).

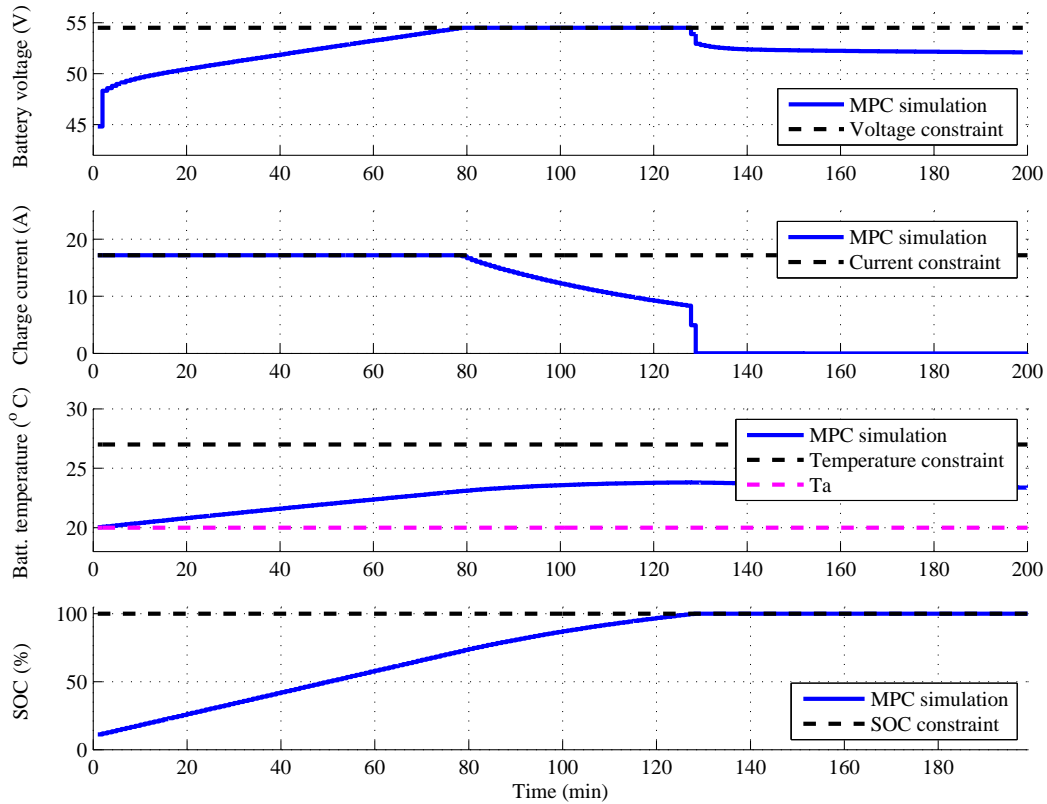


Figure 5: Simulation results: Charging of the battery stack using the MPC algorithm considering the constraints on the maximum voltage of the battery stack, the maximum current, the maximum temperature increase above the ambient temperature and the maximum SOC

4.1. Charging of the VRLA battery stack

The initial voltages of individual batteries in a battery stack are usually somewhat different. Therefore, the ability to measure the voltage of each battery is very important when charging the battery stack to prevent overcharging of individual batteries. In order to show that, experimental results of the MPC algorithm with different initial voltages of the batteries in the battery stack, are shown in Fig. 9.

The voltage of each battery in the stack is different and their behaviours are not the same [12]. Due to various values of the electrolyte saturation in the batteries, the voltage differences are present even in completely new batteries.

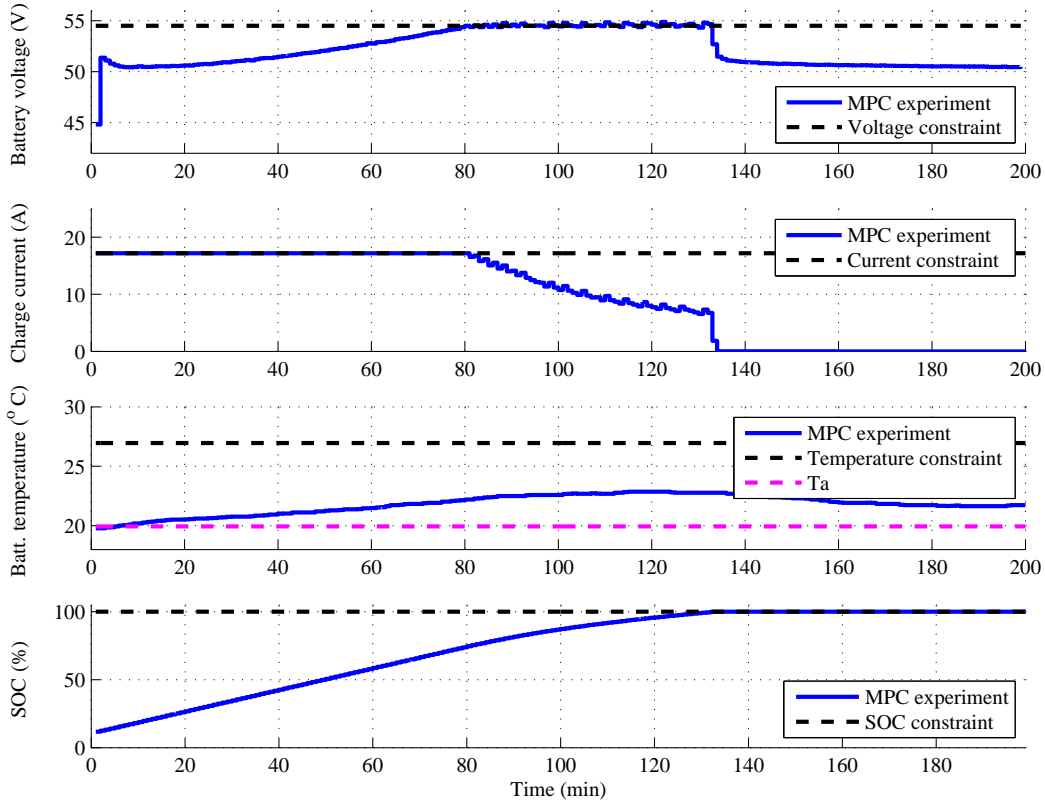


Figure 6: Experimental results: Charging of the battery stack using the MPC algorithm considering the constraints on the maximum voltage of the battery stack, the maximum current, the maximum temperature increase above the ambient temperature and the maximum *SOC*

MPC algorithm keeps the voltage of the battery stack below threshold voltage level (54.50 V) provided by the manufacturer. However, even though the sum of voltages of the individual batteries is below the maximum allowed value, the voltage of some batteries in the stack exceeds the maximum allowed level provided by the manufacturer (13.625 V), as shown in Fig. 9. Batteries which violated this constraint during charging were exposed to an increased oxygen generation and grid corrosion on the positive electrode and to the hydrogen generation on the negative electrode. Named effects cause an increase of the degradation effects within the battery [13], and premature loss of the battery capacity.

The proposed MPC algorithm presented in the previous section can be

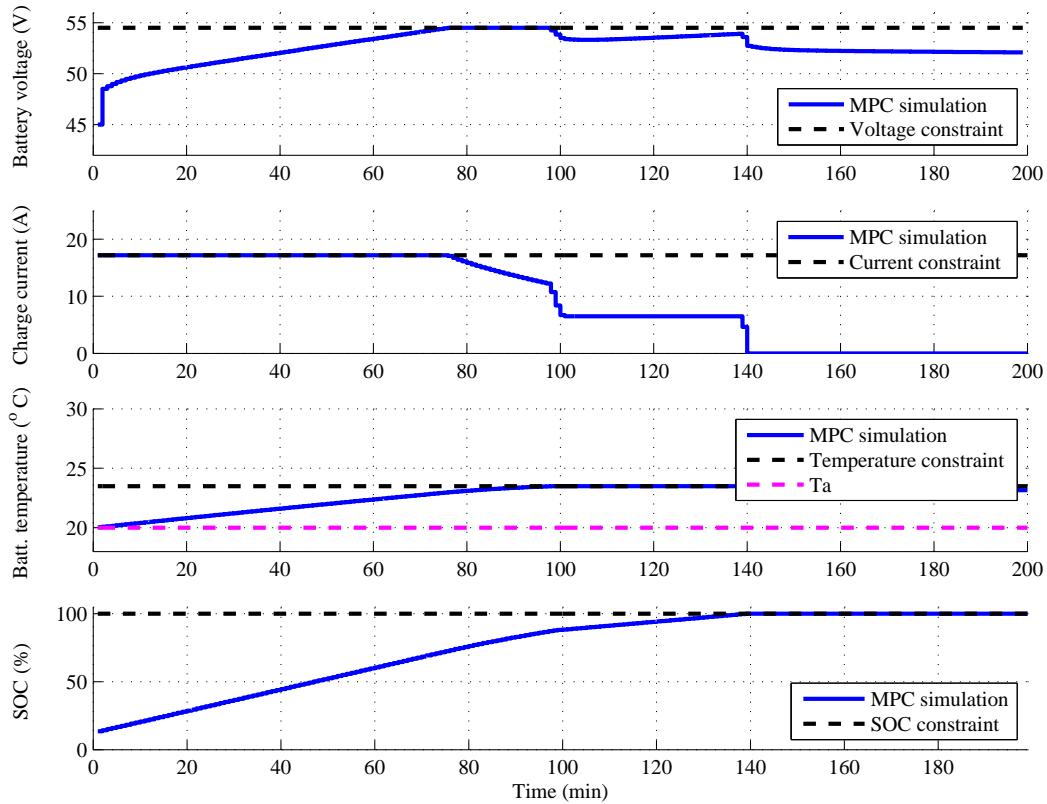


Figure 7: Simulation results: Charging of the battery stack using the MPC algorithm with a lower temperature limit to show that the algorithm is capable of handling the temperature constraint

effectively used for charging VRLA battery stacks by using the hybrid electrical model (2) to model the behaviour of each battery in the stack and by putting additional constraints on the maximum voltage of each battery in the stack ($U_{batti} \leq 13.625$ V). In that way the MPC algorithm has a positive impact on reducing the degradation effects in the battery stack.

Application of the MPC algorithm with this additional constraints can slightly extend the charging time of the battery stack, but it can significantly prolong its lifetime.

Figures 10 and 11 shows simulation and experimental results of charging of the battery stack using the MPC algorithm with the aforementioned constraints while Fig. 12 shows the corresponding voltages of the individual batteries in the battery stack. The MPC algorithm decreases the charge cur-

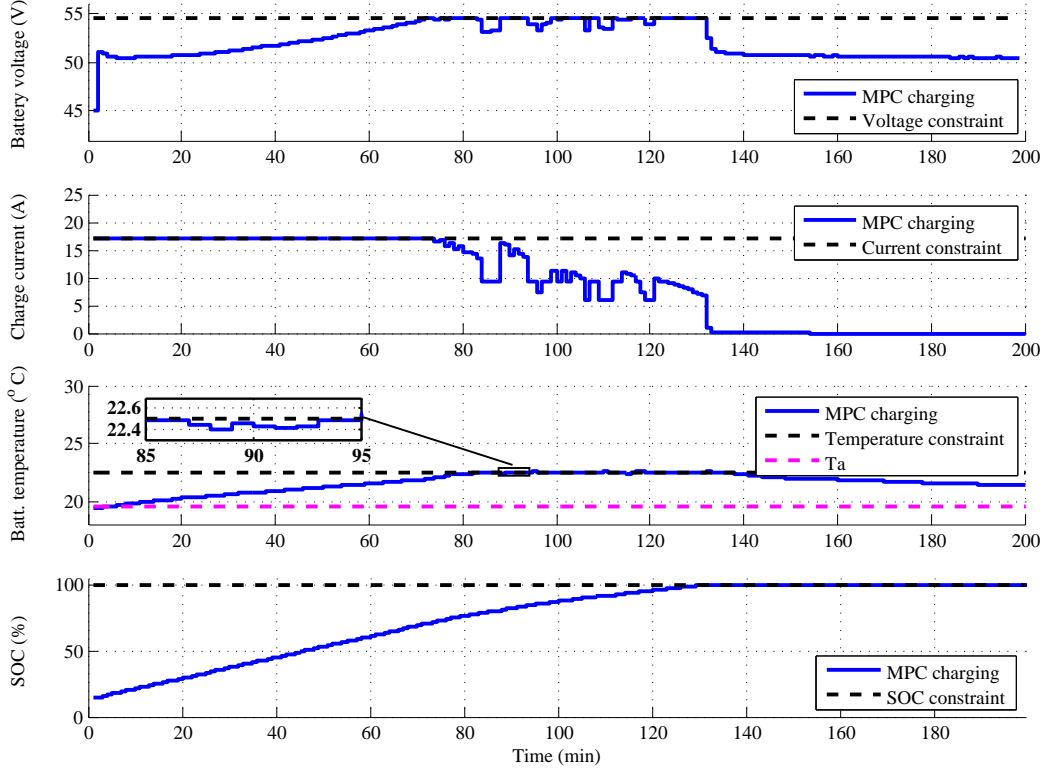


Figure 8: Experimental results: Charging of the battery stack using the MPC algorithm with a lower temperature limit to show that the algorithm is capable of handling the temperature constraint

rent (figures 10 and 11) when the battery voltages in Fig. 12 become close to the maximum allowed value. It can be seen that the battery with the highest voltage value did not violate the voltage constraint in simulation while in the experiment individual batteries slightly violate the aforementioned constraints. However, the violation of the constraints is not significant and it happens due to discrepancy between the battery model and the experimental setup. It can be concluded that the MPC algorithm keeps the battery voltage, temperature and current within the safe limits and can be effective in reducing battery degradation effects and prolonging the battery lifetime.

5. Conclusion

In this paper a new charging method for VRLA batteries based on MPC is proposed. The hybrid equivalent circuit electrical model together with

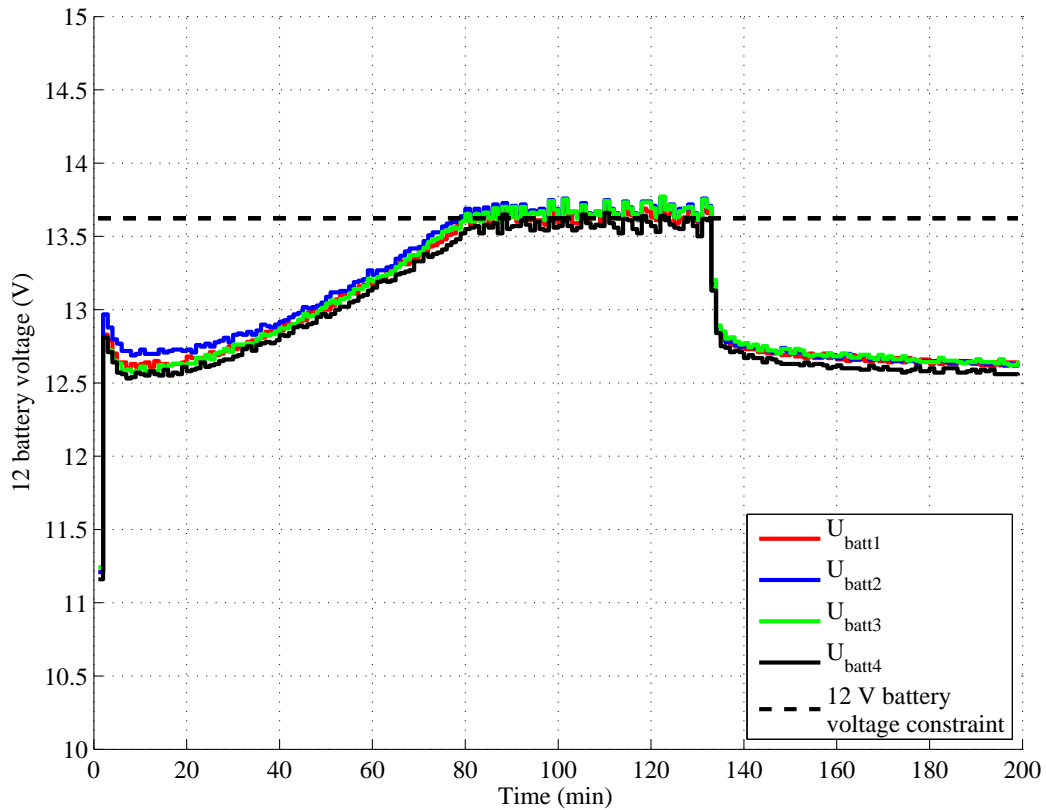


Figure 9: Experimental results: By imposing constraint on the maximum voltage of the battery stack (54.5V) does not necessarily prevent the voltage constraint violation for every battery in the stack (13.625V)

the temperature model are used in the algorithm for prediction of the future behavior of the battery, where the hybrid electrical model is converted to a non-minimal state-space realization in order to avoid using a full-state observer. Even though the presented charging method is developed for charging of VRLA batteries it can be easily adapted to other types of batteries represented by an equivalent circuit model.

The objective of the control algorithm was to charge the battery as fast as possible without violating the following constraints: manufacturer upper threshold voltage level, the maximum battery temperature increase - compared to the ambient temperature, the maximum charge current and the maximum *SOC*. The proposed charging algorithm is proved to be convex, recursively feasible and the closed-loop stability is guaranteed.

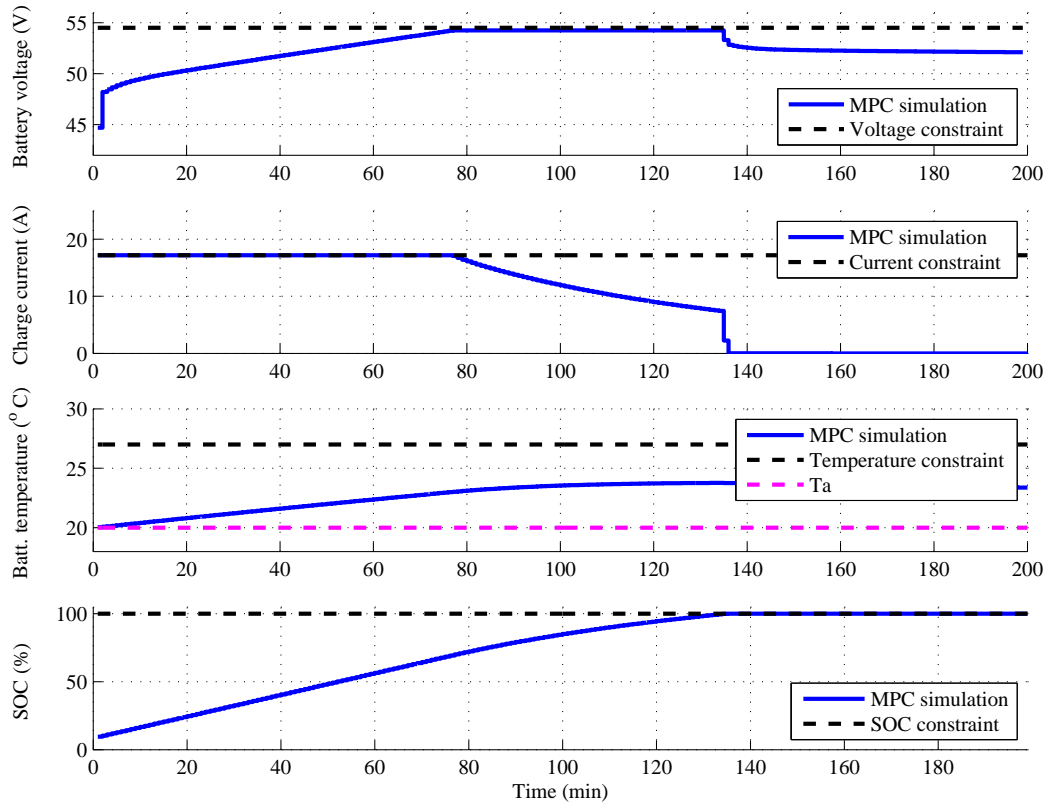


Figure 10: Simulation results: Charging of the battery stack taking into account that the maximum allowed voltage for every battery in the stack is less than 13.625 V

The constraints provided by the manufacturer (a relatively low recommended current), caused that the presented results fully resemble the CCCV method since the maximum temperature constraint was not reached. The charging was driven solely by the maximum current and the maximum voltage constraint. By relaxing the constraints provided by the manufacturer (allowing a higher charge current), the battery temperature limit would become an important issue during charging. To show that the algorithm can cope with such a case, the temperature constraint was tightened. The algorithm adjusted the charging current to respect a tightened temperature constraint.

In addition, the MPC algorithm is extended for charging the VRLA battery stack by taking into account the maximum allowed voltage of individual batteries in the battery stack. The simulation and experimental results

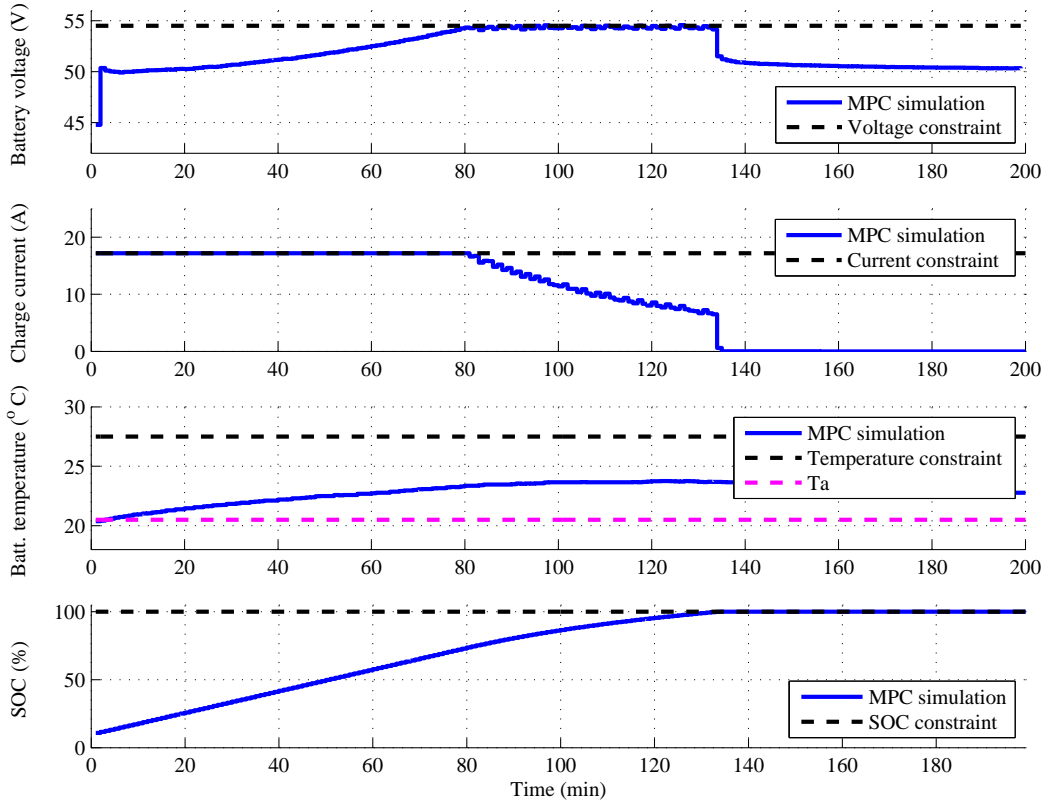


Figure 11: Experimental results: Charging of the battery stack taking into account that the maximum allowed voltage for every battery in the stack is less than 13.625 V

showed that the proposed MPC algorithm managed to charge the battery taking into account all the aforementioned constraints.

The main benefit of using the proposed MPC algorithm compared to standard CCCV method is in its ability to take into account the constraints on the maximum temperature and the maximum voltage of individual batteries in the battery stack. If a single battery is charged and the battery temperature is not an issue during charging, there is no difference between the proposed algorithm and the CCCV method. However, the constraints in the MPC algorithm can be set according to the new knowledge about influence of the constraints on the battery lifetime, still providing the aforementioned guarantees.

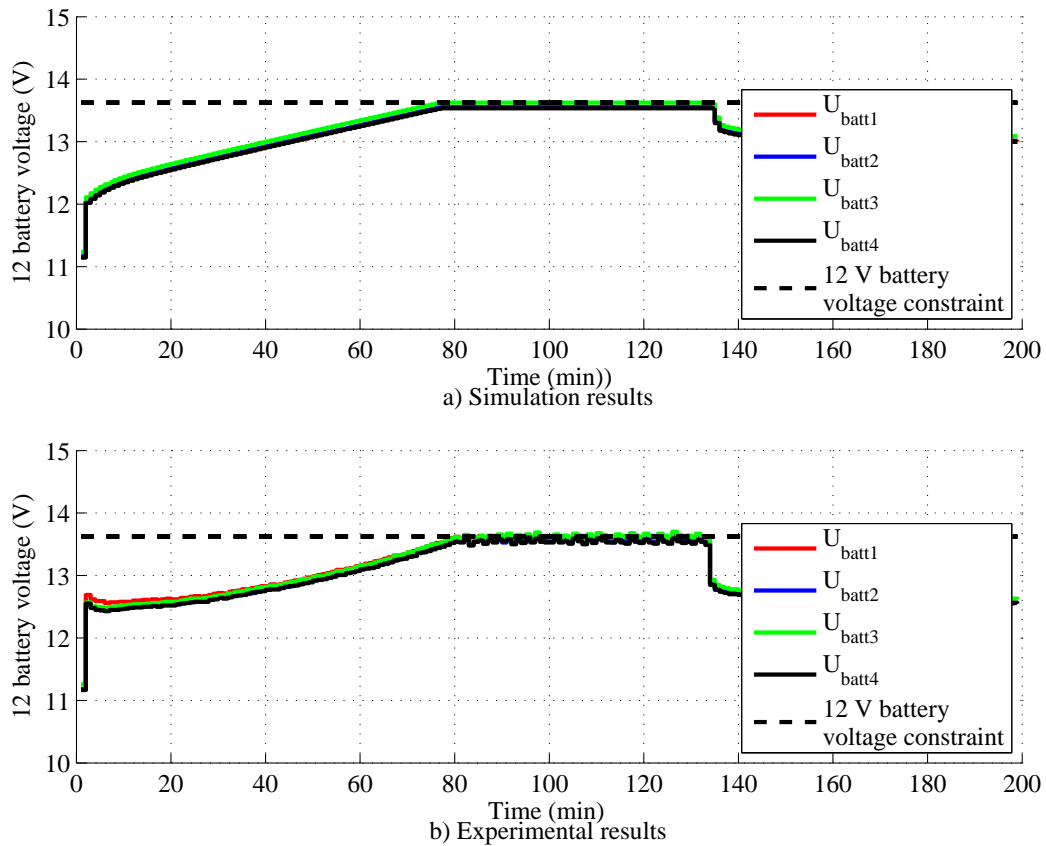


Figure 12: The voltages of the batteries used in the battery stack during charging with the MPC algorithm taking into account the maximum allowed voltage for every battery in the stack: Simulation and experimental results

References

- [1] B. Culpin, Separator design for valve-regulated lead/acid batteries, *Journal of Power Sources* 53 (1) (1995) 127–135.
- [2] D. W. Lambert, P. H. Greenwood, M. C. Reed, Advances in gelled-electrolyte technology for valve-regulated lead-acid batteries, *Journal of Power Sources* 107 (2) (2002) 173–179.
- [3] P. M. Hunter, A. H. Anbuky, VRLA battery rapid charging under stress management, *Industrial Electronics, IEEE Transactions on* 50 (6) (2003) 1229–1237.

- [4] Y. Wong, W. Hurley, W. Wölfle, Charge regimes for valve-regulated lead-acid batteries: Performance overview inclusive of temperature compensation, *Journal of Power Sources* 183 (2) (2008) 783–791.
- [5] X. Wang, A. Palazoglu, N. H. El-Farra, Operational optimization and demand response of hybrid renewable energy systems, *Applied Energy* 143 (2015) 324–335.
- [6] A. Parisio, E. Rikos, G. Tzamalis, L. Glielmo, Use of model predictive control for experimental microgrid optimization, *Applied Energy* 115 (2014) 37–46.
- [7] T. Ikeya, N. Sawada, S. Takagi, J.-i. Murakami, K. Kobayashi, T. Sakabe, E. Kousaka, H. Yoshioka, S. Kato, M. Yamashita, et al., Charging operation with high energy efficiency for electric vehicle valve-regulated lead–acid battery system, *Journal of Power Sources* 91 (2) (2000) 130–136.
- [8] F. Fleming, P. Shumard, B. Dickinson, Rapid recharge capability of valve-regulated lead-acid batteries for electric vehicle and hybrid electric vehicle applications, *Journal of Power Sources* 78 (1) (1999) 237–243.
- [9] V. Svoboda, H. Doering, J. Garche, The influence of fast charging on the performance of VRLA batteries, *Journal of Power Sources* 144 (1) (2005) 244–254.
- [10] R. Dufo-López, J. M. Lujano-Rojas, J. L. Bernal-Agustín, Comparison of different lead–acid battery lifetime prediction models for use in simulation of stand-alone photovoltaic systems, *Applied Energy* 115 (2014) 242–253.
- [11] T. Reddy, *Linden’s Handbook of Batteries*, 4th Edition, McGraw-Hill Education, 2010.
- [12] D. A. J. Parker, P. T. Moseley, J. Garche, C. D. Parker, *Valve-Regulated Lead-Acid Batteries*, Elsevier, Amsterdam, 2004.
- [13] P. M. Hunter, *VRLA battery float charge: analysis and optimisation*, Ph.D. thesis, University of Canterbury, Christchurch, New Zealand (2003).

- [14] E. Rossinot, C. Lefrou, F. Dalard, J. Cun, Batteries in standby applications: comparison of alternate mode versus floating, *Journal of Power Sources* 101 (1) (2001) 27–34.
- [15] E. M. Valeriote, J. Nor, V. A. Ettel, Very fast charging of lead-acid batteries, in: *Proceedings of the 5th International Lead-Acid Battery Seminar*, International Lead Zinc Research Organization (ILZRO), 1991, pp. 93–122.
- [16] R. H. Jones, J. M. McAndrews, F. Vaccaro, Recharging VRLA batteries for maximum life, in: *Telecommunications Energy Conference*, 1998. INTELEC. Twentieth International, IEEE, 1998, pp. 526–531.
- [17] Y. Li, P. Chattopadhyay, A. Ray, Dynamic data-driven identification of battery state-of-charge via symbolic analysis of input–output pairs, *Applied Energy* 155 (2015) 778–790.
- [18] É. Boisvert, Using float charging current measurements to prevent thermal runaway on VRLA batteries, in: *Telecommunications Energy Conference*, 2001. INTELEC 2001. Twenty-Third International, IET, 2001, pp. 126–131.
- [19] R. Klein, N. A. Chaturvedi, J. Christensen, J. Ahmed, R. Findeisen, A. Kojic, Optimal charging strategies in lithium-ion battery, in: *American Control Conference (ACC)*, 2011, IEEE, 2011, pp. 382–387.
- [20] D. Q. Mayne, J. B. Rawlings, C. V. Rao, P. O. Scokaert, Constrained model predictive control: Stability and optimality, *Automatica* 36 (6) (2000) 789–814.
- [21] D. Q. Mayne, Model predictive control: Recent developments and future promise, *Automatica* 50 (12) (2014) 2967–2986.
- [22] J. Silvente, G. M. Kopanos, E. N. Pistikopoulos, A. Espuña, A rolling horizon optimization framework for the simultaneous energy supply and demand planning in microgrids, *Applied Energy* 155 (2015) 485–501.
- [23] J. Li, M. A. Danzer, Optimal charge control strategies for stationary photovoltaic battery systems, *Journal of Power Sources* 258 (2014) 365–373.

- [24] M. Petrollese, L. Valverde, D. Cocco, G. Cau, J. Guerra, Real-time integration of optimal generation scheduling with MPC for the energy management of a renewable hydrogen-based microgrid, *Applied Energy* 166 (2016) 96–106.
- [25] B. Hredzak, V. G. Agelidis, G. Demetriades, Application of explicit model predictive control to a hybrid battery-ultracapacitor power source, *Journal of Power Sources* 277 (2015) 84–94.
- [26] J. Yan, G. Xu, H. Qian, Y. Xu, Z. Song, Model predictive control-based fast charging for vehicular batteries, *Energies* 4 (8) (2011) 1178–1196.
- [27] M. A. Xavier, M. S. Trimboli, Lithium-ion battery cell-level control using constrained model predictive control and equivalent circuit models, *Journal of Power Sources* 285 (2015) 374–384.
- [28] M. Torchio, N. A. Wolff, D. M. Raimondo, L. Magni, U. Kreuer, R. B. Gopaluni, J. A. Paulson, R. D. Braatz, Real-time model predictive control for the optimal charging of a lithium-ion battery, in: *American Control Conference (ACC)*, 2015, IEEE, 2015, pp. 4536–4541.
- [29] P. Fortenbacher, J. L. Mathieu, G. Andersson, Modeling, identification, and optimal control of batteries for power system applications, in: *Power Systems Computation Conference (PSCC)*, 2014, IEEE, 2014, pp. 1–7.
- [30] J. Löfberg, Oops! I cannot do it again: Testing for recursive feasibility in MPC, *Automatica* 48 (3) (2012) 550–555.
- [31] P. E. Pascoe, A. H. Anbuky, A VRLA battery simulation model, *Energy Conversion and Management* 45 (7) (2004) 1015–1041.
- [32] M. Chen, G. A. Rincon-Mora, Accurate electrical battery model capable of predicting runtime and I–V performance, *Energy Conversion, IEEE Transactions on* 21 (2) (2006) 504–511.
- [33] M. Kulkarni, V. D. Agrawal, Energy source lifetime optimization for a digital system through power management, in: *System Theory (SSST)*, 2011 IEEE 43rd Southeastern Symposium on, IEEE, 2011, pp. 73–78.
- [34] H. Rahimi-Eichi, U. Ojha, F. Baronti, M.-Y. Chow, Battery management system: an overview of its application in the smart grid and electric vehicles, *Industrial Electronics Magazine, IEEE* 7 (2) (2013) 4–16.

- [35] T. Dragičević, Hierarchical control of a direct current microgrid with energy storage systems in a distributed topology, Ph.D. thesis, Faculty of Electrical Engineering and Computing, University of Zagreb (2013).
- [36] D. Doerffel, S. A. Sharkh, A critical review of using the Peukert equation for determining the remaining capacity of lead-acid and lithium-ion batteries, *Journal of Power Sources* 155 (2) (2006) 395–400.
- [37] FIAMM, Installation&Operating Instructions, Technical Manual VRLA, <http://www.blueboxbatteries.co.uk/brands/fiamm/flb/dyn/filemanager/fiamm-installation-operating-manual-from-blue-box.pdf>, [Online; accessed 13-August-2016].
- [38] B. S. Bhangu, P. Bentley, D. A. Stone, C. M. Bingham, Nonlinear observers for predicting state-of-charge and state-of-health of lead-acid batteries for hybrid-electric vehicles, *IEEE Transactions on Vehicular Technology* 54 (3) (2005) 783–794.
- [39] P. T. Krein, R. S. Balog, Life extension through charge equalization of lead-acid batteries, in: *Telecommunications Energy Conference, 2002. INTELEC. 24th Annual International*, IEEE, 2002, pp. 516–523.
- [40] D. A. Kölbl, Parameters to consider for installation of VRLA-batteries versus different ambient temperatures, in: *Annual International Telecommunications Energy Conference, 2002*, pp. 530–532.
- [41] E. Vaccaro, J. Rhoades, A. B. Le, VRLA battery temperature concerns other than just thermal runaway. I. Practical considerations, in: *Telecommunications Energy Conference, 1996. INTELEC'96., 18th International*, IEEE, 1996, pp. 39–44.
- [42] D. Berndt, Valve-regulated lead-acid batteries, *Journal of Power Sources* 100 (1) (2001) 29–46.
- [43] Ritar, RA 12-45, <http://www.nps.com.au/wp-content/uploads/2013/10/RA12-45.pdf>, [Online; accessed 10-December-2015] (1).
- [44] Delta, PSC 3 telecom power system controller, <http://www.rectifier.co.za/Delta/psc-3-tds.pdf>, [Online; accessed 10-December-2015] (1).

- [45] S. Abu-Sharkh, D. Doerffel, Rapid test and non-linear model characterisation of solid-state lithium-ion batteries, *Journal of Power Sources* 130 (1) (2004) 266–274.
- [46] G. Kujundžić, M. Vašak, J. Matuško, Estimation of VRLA Battery States and Parameters using Sigma-point Kalman Filter, in: *International Conference on Electrical drives and power electronics (18; 2015); Joint Slovak-Croatian Conference (7; 2015)*, 2015.
- [47] E. K. P. Chong, S. H. Żak, *An Introduction to Optimization*, 2nd Edition, A Wiley-Interscience Publication, John Wiley&Sons Inc., 2001, pp. 187–217.
- [48] P. O. Sokaert, J. B. Rawlings, E. S. Meadows, Discrete-time stability with perturbations: Application to model predictive control, *Automatica* 33 (3) (1997) 463–470.
- [49] J. Pannek, M. von Lossow, Stability of observer based predictive control for nonlinear sampled-data systems, *arXiv preprint arXiv:1105.3272*.
- [50] J. Löfberg, YALMIP: A toolbox for modeling and optimization in Matlab, in: *Computer Aided Control Systems Design, 2004 IEEE International Symposium on*, IEEE, 2004, pp. 284–289.
- [51] J. F. Sturm, Using SeDuMi 1.02, a MATLAB toolbox for optimization over symmetric cones, *Optimization methods and software* 11 (1-4) (1999) 625–653.
- [52] M. Herceg, M. Kvasnica, C. Jones, M. Morari, Multi-parametric toolbox 3.0, in: *Proceedings of the European control conference*, no. EPFL-CONF-186265, 2013.